http://dx.doi.org/10.21577/0103-5053.20190109

J. Braz. Chem. Soc., Vol. 30, No. 10, 2182-2190, 2019
Printed in Brazil - ©2019 Sociedade Brasileira de Química

Article

Catalytic Transformation Conditions of Ethanol on Dealuminated BEA Zeolites

Maria Clara H. Clemente,[a] Deborah S. Valadares,[a] André B. Lacava,[a] Lais S. Barbosa,[a] Gesley A. V. Martins,[a] José A. Dias[a] and Sílvia C. L. Dias[*,a]*

[a]*Laboratório de Catálise, Instituto de Química, Universidade de Brasília, Campus Universitário Darcy Ribeiro, Asa Norte, 70910-900 Brasília-DF, Brazil*

Catalysis is an important tool in obtaining a range of derivative products from renewable sources, such as ethanol. Solid-state dealumination using ammonium hexafluorosilicate on the BEA zeolite under the treatment at temperature of 190 °C, 70 mol% dealumination in the presence of humidity and washing with buffer solution at 25 °C generated larger pores. The absence of washing procedure for the same sample resulted in pore blockage. Ethanol dehydration reactions showed conversion of 72% (64% ethylene and 8% diethyl ether) for this sample at 300 °C and high weight hourly space velocity (WHSV, 3247 h^{-1}), whereas, at the same temperature but at a low WHSV (57 h^{-1}), the conversion was 88% (49% ethylene and 39% diethyl ether). Dealuminated BEA zeolite presented better diffusion conditions, higher hydrophobicity and generated larger pores. Impregnation with $H_3PW_{12}O_{40}$, $H_4SiW_{12}O_{40}$ and Nb_2O_5 explained the selectivity, showing that Lewis acid sites from Nb_2O_5 favored the diethyl ether production.

Keywords: BEA zeolite, solid-state dealumination, hierarchically structured catalysts, ethanol dehydration, weight hourly space velocity (WHSV) selectivity effect

Introduction

The demand for chemicals, such as aromatics and light olefins produced by sustainable catalytic processes, is of paramount importance in modern chemistry.[1] Particularly, acid-catalyzed alcohol dehydration is a great alternative reaction for olefins' production, leading to reduction of greenhouse gas emissions.[2] It is also commonly used as a model reaction for studying catalytic response of materials.[3-5] Brazil is one of the global leaders in ethanol production, and the building of large-scale plants for the manufacture of polyethylene and other polymers from ethanol is an effective low-carbon-footprint alternative to steam cracking of hydrocarbons.[6-9]

Intramolecular dehydration to ethylene and intermolecular reaction to derive diethyl ether can take place in a competitive way during ethanol dehydration, diethyl ether being favored at low temperatures, and ethylene being favored at high temperatures.[10] Literature reviews[11-13] indicate that higher conversions and better catalytic stability can be obtained for dealuminated zeolites due to the tuning of hydrophobicity, diffusion effect and acidity. Studies of Pál-Bórbély and Beyer[14] reported different methodologies for solid-state dealumination for Y zeolite using ammonium hexafluorosilicate (AHFS) and they suggested that additional silanol groups are created due to the formation of HF in the presence of water. Besides, Pires *et al.*[15] studied the reaction time of dealumination in solid state for Y zeolite and observed that after 2 h of reaction, parallel reactions with complex mechanisms could be responsible for the increase in Si/Al ratio, porosity and hydrophobicity. Nash *et al.*[16] suggested that Brønsted acidic sites are more active than Lewis acidic sites for ethylene with an alcohol feed mixture for dehydration reaction in the following order: HZSM-5 > SAPO-34 > Al-MCM-41 > Zr-KIT-6.

BEA zeolite presents high adsorptive capacity, which makes it much studied in several applications in catalysis[17-19] and selective adsorption/desorption of molecules,[20-22] but the dealumination process is less explored. Thus, in the current work, we disclose the beneficial effect of post-synthetic solid-state dealumination of BEA zeolite to generate hierarchical zeolitic structures within the crystallites for the dehydration of ethanol. Moreover, the effect of dehydration reaction conditions on the selectivity was explored by varying the weight hourly space velocity (WHSV). Also, impregnation of heteropolyacids and niobium into dealuminated BEA zeolite was evaluated to verify the effect in conversion and selectivity.

*e-mail: scdias@unb.br; silviadiasunb@gmail.com

Experimental

Modification of BEA zeolites

Zeolite NH_4BEA, obtained from Zeolyst (mole ratio, SiO_2/Al_2O_3 = 25), underwent dealumination through the solid-state reaction using ammonium hexafluorosilicate, AHFS (Aldrich) at two mol percentages (10 and 70 mol%). After mechanically mixing the solids, the sample was kept for 20 h in: (*i*) a desiccator (vacuum of 200 mmHg and 3A molecular sieves); or (*ii*) a high moisture environment (closed container with saturated solution of ammonium chloride, at atmospheric pressure). The Teflon® receptacle containing the mixture was covered and immediately put in a muffle at two temperatures (150 and 190 ºC) for 3 h. Some washing procedures were tested: (*i*) using ammonium acetate buffer solution at room temperature; (*ii*) with ammonium acetate buffer solution heated to 80 ºC; (*iii*) using distilled water heated to 80 ºC; and (*iv*) without washing procedure. Aliquots of 25 mL of the chosen solutions were used until NaOH test indicated complete absence of aluminum in the washing solution and pH stabilization (average total volume of 250 mL). Finally, an amount of 100 mL of distilled water was added to the mixture to achieve uniform final condition for all samples. Resultant paste mixture was dried at 120 ºC (14 h), ground and calcined at 550 ºC for 8 h (heating ramp at 10 ºC min^{-1}).

The code HB(T)d.h.w was used to identify samples: HB is related to BEA zeolite in protonic form; T is the dealumination temperature; d is the degree of dealumination; h represents the moisture exposure represented alphabetically (R for room environment, D for dry and H for humid); and w indicated information about washing procedure (HW for hot water, HB for hot buffer, RB for buffer at room temperature and NW for no washing). For example, HB(190)70.H.RB means protonic BEA, 70 mol% dealuminated at 190 °C under exposure to humidity and washed with buffer solution at room temperature. For simplicity, after impregnation, the samples were distinguished with the suffix BD70, for example, when the dealuminated sample of HB(190)70.H.RB impregnated with 25 wt.% of $H_3PW_{12}O_{40}$ (HPW), it was nominated 25HPW/BD70; when impregnated with 25 wt.% of $H_4SiW_{12}O_{40}$ (HSiW), it was nominated 25HSiW/BD70; when impregnated with 25 wt.% of Nb_2O_5, it was nominated 25Nb/BD70. The impregnation was performed in an aqueous acid solution (0.1 mol L^{-1} HCl) containing the desired amount of heteropolyacid, HPA (HPW or HSiW, Aldrich, > 99.9%) stirred at 80 °C till the solvent evaporated completely. Finally, the catalysts were ground and calcined at 300 °C for 4 h. For the niobium impregnation, an aqueous solution of ammonium niobium oxalate (Companhia Brasileira de Mineração e Metalurgia (CBMM), Brazil) was added to BD70 and kept at 80 °C till evaporation was complete, and the remaining solid was calcined at 550 °C for 8 h.

Characterizations

X-ray diffraction data (XRD) were obtained in a Bruker powder diffractometer (model D8 Focus, θ-2θ) with radiation from a copper tube (Kα 1.5406 Å), operating at 40 kV and 30 mA at a scanning rate of 2 degree min^{-1} (2θ from 2 to 50°, step of 0.02°).

A Thermo Scientific spectrometer (Nicolet, model 6700) was used to obtain Fourier transform infrared spectroscopy (FTIR) spectra of the structural region of the samples (128 scans and 4 cm^{-1} spectral resolution). Each sample was prepared with a mixture of 1:100 wt.% sample/KBr. The data was analyzed by OPUS® software from Bruker.

Adsorption isotherms of the samples were obtained with a surface area and porosimetry analyzer (Micromeritics, ASAP 2020C) based on physisorption of gaseous N_2 at –196 °C. Before the analysis, samples were degassed with evacuation (target pressure of 10 μm Hg) at 300 °C for 4 h. The equations of BET (Brunauer, Emmet and Teller) in the range of partial pressure (P/P_0) from 0 to 0.1, t-plot method and BJH (Barrett, Joyner and Halenda) were used to describe the experimental isotherms.

The crystallinity (nominated C, in percentage) was obtained by comparison of the XRD pattern of dealuminated HBEA and the standard HBEA, calculated by integration of area under peaks (2θ from 5 to 50°), according to the equation:

$$C \text{ (in percentage)} = [\Sigma \text{ dealuminated zeolite peaks} / \Sigma \text{ HBEA peaks}] \times 100 \quad (1)$$

The relative microporosity in the structure (nominated M, in percentage) was also provided by the volume of N_2 adsorbed (at low relative pressures) by the sample with the adsorbed N_2 volume of a standard (NH_4BEA, in this case), according to literature.[23]

Energy dispersive X-ray fluorescence (EDXRF) spectrometer from Shimadzu (model EDX 720) was employed to determine the quantities of silicon and aluminum atoms. The equipment uses rhodium (Rh) as X-ray target. The samples were prepared with polypropylene film and were analyzed under vacuum.

Solid-state ^{27}Al magic angle spinning nuclear magnetic resonance (MAS NMR) spectra (156.4 MHz) were

obtained in a Bruker Avance III HD Ascend 600 MHz spectrometer (14.1 T and 4 mm CP/MAS probe) with 10 kHz spin rate, 0.4 μs pulse duration and 1 s pulse interval. About 2000 acquisitions for each spectrum were made. The external reference was solid $[Al(H_2O)_6]Cl_3$ (δ 0 ppm).

Acidity was measured by pyridine adsorption. Before gaseous pyridine (Py) adsorption, each sample (ca. 20 mg) was placed in an aluminum crucible and inserted into a glass tube inside a tubular furnace (Thermolyne, model F21100). The catalysts were dehydrated in dried N_2 flow (100 mL min^{-1}) at 300 ºC for 1 h. Then, the system was cooled to 150 °C to initiate gaseous Py passage through samples for 1 h. After that, the temperature was held at 150 °C in a N_2 environment for 1 h to remove any physically adsorbed Py. Immediately after cooling the system, each sample was analyzed using thermal analysis and FTIR (sample was prepared with a mixture of 10:100 wt.% sample/KBr). Thermogravimetric (TG) and derivative thermogravimetric (DTG) curves were obtained with simultaneous TG-DSC system (TA Instruments, model SDT 2960) under the conditions of rising temperature, from room temperature up to 1000 ºC at a heating rate of 10 ºC min^{-1}, and in a nitrogen flow of 100 mL min^{-1}.

Elemental analyses were conducted to quantify the amount of coke formed after the dehydration reaction. The analyses were performed in a CHN system (PerkinElmer, series II, model 2400). Each sample of 2.5 mg was weighed out in tin folding crucibles using a PerkinElmer AD-6 Autobalance (electronic ultra-microbalance with sensitivity of 0.1 μg).

Ethanol dehydration reaction

First, the influence of the BEA zeolite modification after dealumination in the ethanol dehydration reaction was tested with a flame ionization detector (Shimadzu GC-FID, model 2010; Restek Rtx phase-Wax® column with dimensions of 30 m × 0.25 mm × 0.25 μm) in a pulsed-flow fixed-bed microreactor coupled to a gas chromatograph system. An amount of 10.0 mg of the sample (in the form of pellets of dimensions between 355 and 710 μm) was placed inside the reactor and activated at 300 °C for 15 min. A sequence of 10 injections of ethanol (previously dried with 3A molecular sieves) was performed at a reaction temperature of 300 °C. The experimental programming conditions were: pressure of 146.1 kPa, total flow of 231 mL min^{-1}, column flow of 2.24 mL min^{-1}, linear velocity of 44 cm s^{-1}, purge flow of 5 mL min^{-1} and split ratio of 100; temperature of the column at 70 °C for 2.25 min. Helium was the carrier gas, and the flame (FID) temperature was 250 °C. The catalyst was treated *in situ* at 300 °C for 20 min. WHSV was calculated by assuming: the mass feed at 0.079 mg (0.1 μL) of ethanol; contact time was calculated from helium gas flow as 226 mL min^{-1}, and the volume of ethanol in gas phase (ideal gas) at 300 °C, reaching 2.4×10^{-6} h and 10 mg of catalyst. The calculated WHSV was about 3247 h^{-1}.

The supported samples of the best dealuminated zeolite were tested in the same model reaction, but under the following conditions. Firstly, to identify and confirm the products of ethanol dehydration, a programmed reaction temperature system from Altamira Instruments (AMI-90R) coupled to a Dycor Ametek mass spectrometer (0-100 m/e) with continuous and simultaneous detection in eight channels was used. The catalyst (10 mg) was placed in an "U" quartz reactor attached to the equipment and pretreated at 250 °C for 30 min with a heating ramp of 10 °C min^{-1} under argon (Ar) flow at 5 cm^3 min^{-1}. A pulse of 1 μL of ethanol was injected into the system while maintaining the same Ar flow during the reaction at 250 and 300 °C. The reaction products were checked via their respective mass fragments (m/e): 18 (base peak of water), 28 (base peak of ethylene), 29 and 44 (base peak and 80% peak of acetaldehyde, respectively), 31 and 45 (base peak and 55% peak of ethanol, respectively), and 59 and 74 (80% and 50% peak of diethyl ether, respectively). The pattern of fragmentation by electron ionization was followed and compared to the National Institute of Standards and Technology (NIST) mass spectrometry data center. Every care was taken to determine, in separate experiments, the possible peaks from the pattern of fragmentation of other common products (e.g., CO, CO_2) to make the unequivocal assignment.

To study the catalyst lifetime on ethanol dehydration (from 1 up to 50 pulses), tests were performed in a pulse microreactor coupled to a gas chromatography system (2010 Shimadzu, GC-FID) with a Shimadzu CBP1 PONA-M50-042 column (50 m × 0.15 mm × 0.33 μm). In each analysis, 0.5 μL of ethanol was injected into the liner (reactor) containing 10 mg of the catalyst. The experiments were performed under the following conditions: pressure at 95.6 kPa, total flow of 6 mL min^{-1}, column flow of 0.1 mL min^{-1}, linear velocity of 6.4 cm s^{-1}, purge flow of 1 mL min^{-1}, and split ratio of 49; temperature of the column at 35 °C for 26 min. Helium was the carrier gas, and the flame (FID) temperature was 250 °C. The catalyst was treated *in situ* at 250 °C for 30 min. WHSV was calculated to be about 57 h^{-1} on the assumption that the mass feed was 0.394 mg (0.5 μL) of ethanol; contact time was calculated from helium gas flow (5 mL min^{-1}) and the volume of ethanol in gas phase (ideal gas) at 300 °C,

reaching 6.9×10^{-4} h; 10 mg of catalyst were used. All chromatographic results were also compared to standard substances (ethylene, diethyl ether and acetaldehyde) to confirm the retention times.

Results and Discussion

Structural characterization

Sample diffractograms (Figure S1 in the Supplementary Information (SI) section) and infrared spectra (Figure S2 in the SI section) indicated that the zeolite structure was preserved, irrespective of the applied dealumination method. The infrared band of symmetrical stretching of all dealuminated samples slight shifted to higher frequencies, which is consistent with dealumination.[24] Sample HB(190)70.H.NW was the one that presented the largest displacement, an indicative of a higher degree of dealumination.[25]

Isotherms of N_2 adsorption (Figure S3 in the SI section) and the textural parameters (Table S1 in the SI section) were obtained for all samples confirming the predominance of microporous structure for these zeolites. Textural analysis results (Figure 1) showed that majority of the samples presented a trend of slightly decrease in the total surface area (sum of micro, meso and external areas). Except for the HB(190)70.H.NW, the mesoporous and external areas showed a minor increase, while microporous area showed a slight decrease.

The micropore structure[23] remained the same for most samples (Table 1, column 2), whereas the crystallinity (Table 1, column 3) slight decreased as observed by XRD data. The unwashed HB(190)70.H.NW sample showed

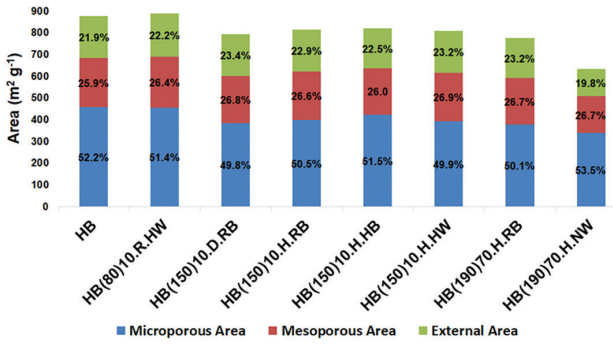

Figure 1. Distribution of areas for HB and dealuminated HB, with external surface area obtained by t-plot method, microporous surface area was obtained by the subtraction of BET specific surface area from t-plot external surface area, and mesoporous surface area obtained from BJH method.

a considerable formation of extra-framework aluminum (EFAL) species, resulting in the blockage of pores and low crystallinity value (Table 1 and Figure 2).[26] The distribution of meso and microporous areas (Figure 1) was practically the same for most samples (except for HB(190)70.H.NW).[19,27] This fact, in addition to the preservation of high crystallinity (Table 1), may indicate that the dealumination by exchange of Al by Si atoms was effective since a significant increase in mesoporous area was not detected (a typical tendency seen in classic dealumination by water vapor or acid solutions).

It is also interesting that HB(190)70.H.NW maintained practically the same meso and microporous proportion (Figure 1), an evidence that EFAL species formation occurred in a homogeneous manner in the zeolite structure (Figure 3). The total area decreased in all distributions of dealuminated samples with a small decrease in the external area distribution (from 21.9 to 19.8%), and consequently

Table 1. Crystallinity, textural data and average Si/Al ratio for NH_4B, HB and dealuminated catalysts

Catalyst	M[a] / %	C[b] / %	D_m[c] / nm	V_μ[d] / (cm^3 g^1)	Si/Al[e] ratio / (mol_{Si} mol_{Al}^{-1})
NH_4B	106	82	9.1	0.18	12.5 ± 0.1
HB	100	100	11.4	0.18	12.4 ± 0.3
HB(80)10.R.HW	121	84	10.8	0.18	15.7 ± 0.2
HB(150)10.D.RB	108	77	11.3	0.17	13.7 ± 0.3
HB(150)10.H.RB	115	74	10.9	0.18	13.2 ± 0.1
HB(150)10.H.HB	107	93	10.5	0.17	13.2 ± 0.1
HB(150)10.H.HW	108	93	11.7	0.17	15.1 ± 0.2
HB(190)70.H.RB	112	87	12.5	0.17	18.7 ± 0.1
HB(190)70.H.NW	94	83	9.1	0.14	14.3 ± 0.1

[a]M: relative microporosity obtained with adsorption capacity data from reference 23; [b]C: relative crystallinity obtained by X-ray diffraction (XRD); [c]D_m: average mesoporous diameter obtained by BJH (Barrett, Joyner and Halenda) method; [d]V_μ: microporous volume obtained by t-plot method; [e]average Si/Al ratio obtained by energy dispersive X-ray fluorescence (EDXRF) technique. The reference value given by Zeolyst was Si/Al = 12.5 (in mol_{Si} mol_{Al}^{-1}) for NH_4B.

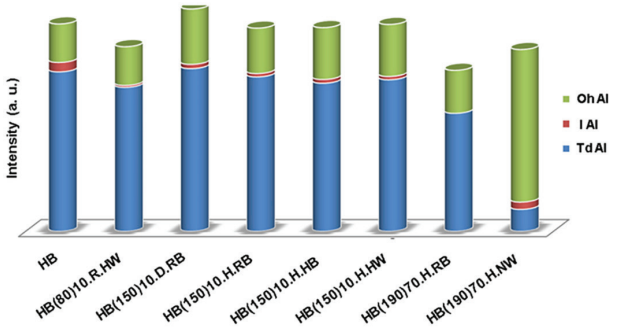

Figure 2. Aluminum environment distribution obtained by the integration of ^{27}Al MAS NMR signals; Td: tetrahedral, I: intermediate (distorted tetrahedral or penta-coordinated), and Oh: octahedral, for aluminum atoms.

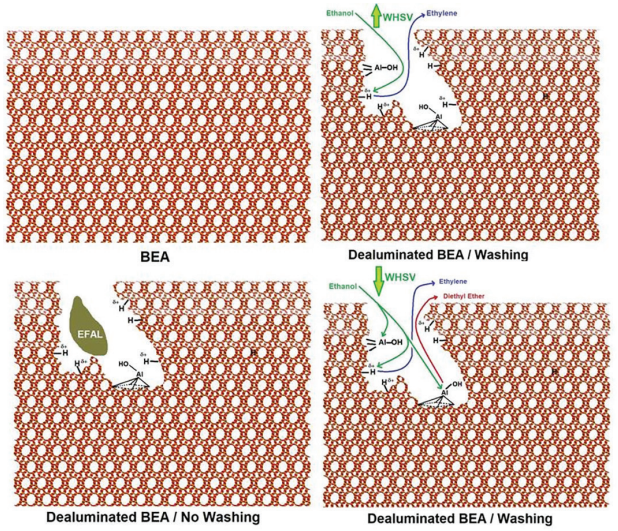

Figure 3. Porous representation of BEA zeolite before and after reaction with ammonium hexafluorosilicate (AHFS), showing the formation of bigger extra-framework aluminum (EFAL) species (no washing) and the product selectivity depending on weight hourly space velocity (WHSV).

increased in microporous area distribution (from 52.2 to 53.5%) for HB(190)70.H.NW in comparison to HB.

The increase in the average mesoporous diameter (D_m) right after calcination of NH_4B (Table 1) could be a consequence of the compensation cation exchange. Besides, sample HB(190)70.H.NW presented the same D_m value as NH_4B, which can be explained as a consequence of the presence of EFAL species that decreased the effective pore space and led to a drop in microporous volume (V_μ). The use of higher temperature and the presence of higher amounts of AHFS in HB(190)70.H.RB seemed to have favored the generation of the larger pores (Table 1) on the resulting hierarchical zeolitic materials.[28,29]

The reason for this might be both the higher temperature and the higher amount of AHFS. The higher temperature could have expanded mesopore diameter and shrunk the pore length (keeping mesoporous area constant). At the same time, AHFS molecules occupied the pores, reacted and generated EFAL species, preserving the expanded mesoporous diameter, even when the system returned to room temperature. The same might have happened to sample HB(190)70.H.NW, but the lack of washing and the consequent pore blockage hid this behavior.

The results of X-ray fluorescence (Table 1) showed that HB(190)70.H.RB presented the highest average Si/Al ratio. It is important to remember that X-ray fluorescence measures the global amount of Si and Al (from framework and extra framework). Thereby, regarding HB(190)70.H.NW, no significant variation was expected in the Si/Al ratio because all the removed Al must remain outside the framework (there was no washing procedure in this methodology). The slight increase in the average Si/Al ratio can be explained simply as the result of the incorporation of the Si atoms provided by AHFS into the structure.

Results of ^{27}Al MAS NMR evidenced that HB(190)70.H.NW was the sample with the lowest amount of tetrahedral aluminum (Figures 2 and S4 in the SI section) and, therefore, the most effective in dealumination (in agreement with literature studies with ZSM-5).[25] Nevertheless, this sample presented an enormous quantity of EFAL species, as can be seen by the presence of large amount of octahedral aluminum (Figure 2), which could have led to low catalytic activity. The results of X-ray fluorescence test showed HB(190)70.H.RB catalyst to be the one with the lowest amount of tetrahedral aluminum. And, therefore, it also had proportionally higher amount of octahedral aluminum compared to HB.

Acid characterization

The sample HB(190)70.H.NW presented the highest Brønsted/Lewis ratio and the lowest number of sites (Table 2). It was expected that this sample would show a low quantity of adsorbed pyridine because this modified zeolite had exhibited greater degree of pore blockage, which resulted in acid sites becoming inaccessible (Figure 3). This blockage could render inaccessible even Lewis acid sites (extra-framework species), and thus, leaving only a small number of acid sites (0.06 mmol g^{-1}) accessible as compared to the other catalysts (ca. 0.5-0.7 mmol g^{-1}).

The majority of dealuminated samples presented a decrease in the amount of acid sites (Table 2), a result commonly found after dealumination process since the loss of a tetrahedral aluminum atom also meant the loss of a Brønsted acid site. A trend of increasing the Brønsted/Lewis acid site ratio after dealumination processes was observed. Also, the decrease in the number of Lewis acid sites seemed to be more pronounced than the

Table 2. Brønsted/Lewis acid site ratio, the number of acid sites (n_{py}), ethanol conversion of the catalysts, and coke formed after ethanol dehydration reaction

Catalyst	Brønsted/Lewis ratio[a]	n_{py}[b] / (mmol g^{-1})	Ethanol conversion[c] / %	Coke[d] / %
HB	1.44	0.70	62	0.2
HB(80)10.R.HW	1.49	0.71	45	0.4
HB(150)10.D.RB	1.89	0.65	44	0.2
HB(150)10.H.RB	2.29	0.69	58	0.3
HB(150)10.H.HB	1.67	0.70	54	0.3
HB(150)10.H.HW	1.70	0.67	54	0.2
HB(190)70.H.RB	1.56	0.49	72	0.6
HB(190)70.H.NW	–	0.06	19	0.2

[a]Ratio obtained by the integration of infrared spectroscopic bands after pyridine adsorption (arbitrary unit); [b]n_{py}: amount of acid sites determined by thermogravimetric (TG) analysis of adsorbed pyridine; [c]ethanol conversion to products (ethylene and diethyl ether) obtained by integration of chromatographic peaks; [d]coke formed on the zeolite after catalytic reaction, measured by elemental analysis.

reduction in the number of Brønsted acid sites, indicating that the drop of acid sites was more dependent on the cleaning of zeolite pores and channels than on the removal of Al from the framework.

Catalytic tests

Dehydration of ethanol to ethylene under high WHSV condition

The catalyst with the best value of ethanol conversion to products, a sample with intermediate amount of acid sites and Brønsted/Lewis acid site ratio, was HB(190)70.H.RB (Table 2). This indicated that the dependency of the acid site total number on the ethanol conversion with: (*i*) was not prominent; (*ii*) it was not linear and could be subject to constructive or destructive interferences coming from other features of the zeolite; and (*iii*) it could be closely related to the catalytic conditions (WHSV).

The hydrophobicity of the sample can be a characteristic very relevant to the reaction[23] because water (one of the byproducts of the reaction) can compete with ethanol for the acid sites. In a more hydrophobic system, such as HB(190)70.H.RB, water can leave from the surface faster, making acid sites more accessible to ethanol. Following the same logic of better diffusion, a larger pore diameter can also have an important role in the catalytic response of this sample as this sample presented the largest pore diameter among the studied catalysts. Therefore, dehydration of ethanol to ethylene by catalysis using dealuminated BEA zeolite seemed to be more dependent on diffusion conditions of molecules than on the number of acid sites. The improvement of the catalytic performance is related to lowering the restriction of the reactant diffusion into the mesopores as BEA zeolite presents improved diffusion due to the absence of cavities (such as, Y zeolite). This possibility is consistent with conclusion that Phung *et al.*[26] drew from a study in which several zeolites were used, namely, that the confinement effects were of importance in ethanol dehydration. However, molecule diffusions cannot be the only activity that influences the mechanism of the ethanol dehydration reaction.

A proof for the above conclusion can be found by comparing samples HB(150)10.D.RB and HB(150)10.H.RB. The modified zeolite, having the favorable characteristics of higher Si/Al ratio (therefore, being more hydrophobic) and with larger pore diameter, presented an inferior catalytic conversion. Considering this, it was more likely that the extent of catalytic dehydration of ethanol depended on a combination of diffusion effects and acidity. The sample HB(190)70.H.RB exhibited the best combination of both the above factors.

Hierarchical' structured zeolites integrate at least two levels (types) of porosity, i.e., micropores and mesopores. They offer a solution to the mass transfer problem associated with conventional zeolites since they couple, in a single material, the catalytic features of micropores and the improved access and transport properties of the additional porosity (mesopores). Hierarchical zeolite crystals can be introduced by the post-synthetic treatment (dealumination) of pre-synthesized BEA crystals.[28]

These results further demonstrate that the use of hierarchically structured zeolites can have very positive effects on the reactions that are limited by intra-crystalline diffusion of the reactants in the mesopores. This joint effect of diffusion and acidity explains why the catalytic response of sample HB(190)70.H.NW was the worst among the samples. The reason was high pore blockage and inaccessibility of the acid sites.

The amount of coke formed in each catalyst after reaction (Table 2) was practically the same, except for

HB(190)70.H.RB, which promoted the highest conversion to ethylene. Usually, for the other catalysts tested by our group for ethanol dehydration, the higher rate of conversion resulted in larger amounts of coke.[30] Regarding catalyst selectivity, it is important to remember that ethanol dehydration can also produce acetaldehyde and light compounds, such as, CO_2, CO and H_2.[7,31,32] However, only ethylene and diethyl ether were detected in the present reaction conditions. Sample HB(190)70.H.RB presented the best value of selectivity for conversion to ethylene, 89%, while HB showed a selectivity of about 78% for the same product (Figure 4).

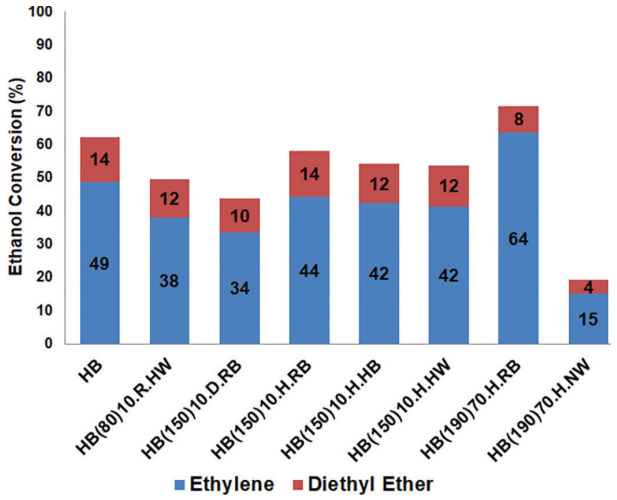

Figure 4. Ethanol conversion and selectivity to ethylene and diethyl ether for dealuminated zeolites, using a pulsed-flow fixed-bed microreactor coupled to a gas chromatograph system at 300 °C (10 pulses, WHSV = 3247 h^{-1}).

Ethanol dehydration to ethylene under low WHSV condition

Once selected, the best dealuminated zeolite BEA (i.e., HB(190)70.H.RB) was tested in the same reaction under various conditions and compared with other synthesized catalysts (Figures S5 and S6). For these tests, the reaction was run at lower WHSV (57 h^{-1}) and monitored from a single pulse up to 50 pulses. According to the rules of thermodynamics, like other chemical reactions, at higher temperatures the dehydration reaction of ethanol to ethylene is driven with greater intensity.[10,33] Therefore, the catalysts were tested at two temperatures: 250 and 300 °C. For simplification, the notation used will be BD70 for HB(190)70.H.RB. Figure 5 shows the ethanol conversion with BD70. HB and various other impregnated catalysts on HB were used for comparison with BD70. We observed that, at higher temperature (300 °C), the reaction was driven to higher ethylene formation in case of most of the catalysts and during every stage of the experiment (from pulse 1 to 50). However, there were a few exceptions.

Despite the results observed under high WHSV conditions, we assumed that dealumination process increases the mesoporous area on the material and produced terminal (≡Al–OH), as shown in Figure 3, when HB and BD70 catalysts are compared. Under high WHSV condition, ethanol molecules preferentially interact with Brønsted acid sites instead of Lewis acid sites since the strongest Brønsted sites have the highest free energy on the catalyst surface.[34] Then, at high WHSV (3247 h^{-1}) conditions, BD70 presented the best result for ethanol to ethylene conversion. On the other hand, at low WHSV (57 h^{-1}), the main product was diethyl ether, which is attributable to different diffusion effects caused by the WHSV parameter. At low WHSV, Lewis acid sites could also be reached, and diethyl ether was produced competitively. This observation was confirmed by the catalytic tests using 25Nb/BD70, which is rich in Lewis acid sites due to niobium species on its surface.[35] Coke also probably plays an important role in the deactivation of catalysts since overall yield decreased (pulse 50), but the selectivity for diethyl ether increased further. This can be attributed to the strength of the Brønsted acid sites, which were probably blocked by coke, making the weaker Lewis sites gain preference and resulting in lesser ethanol conversion and more diethyl ether conversion. It is worth noting that these results showing higher selectivity to diethyl ether generation over BD70, point at WHSV as the effective variable factor for changing reaction conditions in the context of reaction engineering.

Other observations were also obtained for the other catalysts that were tested as supporting catalysts. Initially, the heteropolyacid (HPW and HSiW) supported catalysts, which is known to have an enhanced number of Brønsted sites,[36] produced only ethylene (pulse 1). However, by the time the reaction ran at pulse 50, diethyl ether started forming. This can be attributed to the degradation of the supported heteropolyacid over longer time and at higher temperatures, at which Lewis acid sites may be formed from the oxides.[37]

Interestingly, catalysts 25HPW/BD70 and 25HSiW/BD70 exhibited lower substrate conversion than HB (Figure 5), suggesting the external acid sites of the zeolite crystal are inhibited by the HPA impregnation. It was demonstrated that HPA was impregnated on the external surface of zeolite crystal instead of the internal surface because the HPA crystalline domains are bigger than those of the zeolite HB.[36] Considering that HB and HPA/HB have the same zeolite framework, the superior catalytic activity of HB should be attributed to the hydrophobic surface, which could efficiently enrich the alcohol substrate and keep water away from the acid sites.[38] These features are favorable for the dehydration reactions, thus promoting the shift of

reaction balance to the formation of ethylene. Even after 50 pulses of ethanol, the HB catalyst still showed 100% ethanol conversion and 100% selectivity to ethylene, suggesting that the hydrophobicity of the surface is stable. Olefin yield at 300 °C by HB (100%) was comparable to HPW/$Ce_{0.8}Zr_{0.2}O_2$ (> 99%),[30] which showed the importance of the condition of WHSV to the reaction selectivity.

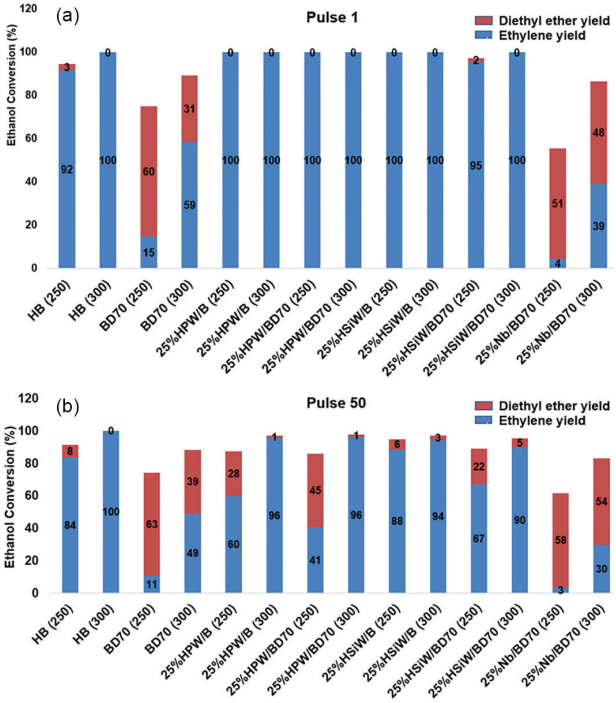

Figure 5. Ethanol conversion and selectivity to ethylene and diethyl ether for the studied catalysts, using a pulsed-flow fixed-bed microreactor coupled to a gas chromatograph system at 250 and 300 °C (1 and 50 pulses, WHSV = 57 h^{-1}).

The effect of dealumination should also be emphasized (Figure 5). The BD70 showed good activity under low WHSV conditions: conversion was 88% (40% diethyl ether and 48% ethylene, at 50 pulses), whereas at high WHSV there was 72% conversion (8% diethyl ether and 64% ethylene, at 10 pulses), both reactions were done at 300 °C. The favorable formation of diethyl ether is even better at 250 °C (69% conversion, 63% diethyl ether and 6% ethylene, after 50 pulses), which is a significant selectivity towards diethyl ether. The selectivity to diethyl ether is also high using niobium supported with BD70 (62% conversion, 58% diethyl ether and 4% ethylene, after 50 pulses). As shown before, the characteristic of these catalysts is that both have an appreciable amount of Lewis acid sites.

Conclusions

Renewable materials are crucial for the sustainability of industries, and catalysis is important for producing cleaner sources of energy by clean processes. In this context, dehydration of ethanol is a key process. So, a series of BEA zeolites were modified and tested for this reaction. Dealuminated BEA zeolites were produced using ammonium hexafluorosilicate (AHFS) under specific conditions. The dealuminated samples maintained their structures over large ranges of temperature and AHFS variations and showed to be effective by producing hierarchical structure in which micro and mesopores were present.

Various dealuminated BEA zeolites were produced and their activities were tested in the ethanol dehydration model reaction, using a pulsed-flow fixed-bed microreactor coupled to a gas chromatograph system (WHSV = 3247 h^{-1}). Treatments at temperature of 190 °C, 70 mol% and dealumination in the presence of humidity and washing with buffer solution at 25 °C produced the best sample with larger pores (HB(190)70.H.RB), and the best results of ethanol dehydration (300 °C, 72% conversion, 64% ethylene and 8% diethyl ether). This sample showed better diffusion conditions (higher hydrophobicity and larger pores), which seemed to be the main reason for the improved catalytic response. Analyzing catalytic behavior of the samples in general, ethylene formation might be related to an optimum point between diffusion factors and Brønsted acidity properties. On the other hand, that catalyst (HB(190)70.H.RB) and other supported ($H_3PW_{12}O_{40}$, $H_4SiW_{12}O_{40}$ and Nb_2O_5) catalysts also were tested under a condition with low WHSV (57 h^{-1}). The results showed a change in the product selectivity (300 °C, 88% conversion, 49% ethylene and 39% diethyl ether) for HB(190)70.H.RB. Dealuminated BEA zeolite presented better diffusion conditions, higher hydrophobicity and larger pores. Coupled with the performance of the other catalysts, it was possible to determine that Lewis acid sites may promote the intermolecular formation preferentially towards diethyl ether, and not towards the intramolecular formation of ethylene.

Thus, these experiments were very significant for demonstrating the importance of the design of a catalyst and the selected reaction conditions. We have shown in ethanol dehydration that, with the use of modified zeolite BEA (protonic, dealuminated and supported), high selectivity for either ethylene or diethyl ether could be achieved. Then, the production of the intended product can be fine-tuned, which showed the versatility of the catalyst under mild conditions, without solvent and on a simple pulse microreactor.

Supplementary Information

Supplementary data are available free of charge at http://jbcs.sbq.org.br as PDF file.

Acknowledgments

We acknowledge Julia M. Muller for collecting data during her doctorate. We also acknowledge CNPq and CAPES for research, doctoral and undergraduate scholarships, as well as UnB/DPI/IQ, FAPDF, CAPES, MCTI/CNPq, FINATEC, FINEP/CTPetro and FINEP/CTInfra for providing financial support. Also, we would like to thank Dr Richieli Vieira (commercial development coordinator, PQ Silicas Brazil) for providing BEA zeolite (CP814E*).

References

1. Centi, G.; Lanzafame, P.; Perathoner, S.; *Catal. Today* **2011**, *167*, 14.
2. Xin, H.; Li, X.; Fang, Y.; Yi, X.; Hu, W.; Chu, Y.; Zhang, F.; Zheng, A.; Zhang, H.; Li, X.; *J. Catal.* **2014**, *312*, 204.
3. Brylewska, K.; Tarach, K. A.; Mozgawa, W.; Olejniczak, Z.; Filek, U.; Góra-Marek, K.; *J. Mol. Struct.* **2016**, *1126*, 147.
4. Matachowski, L.; Zimowska, M.; Mucha, D.; Machej, T.; *Appl. Catal., B* **2012**, *123-124*, 448.
5. Phung, T. K.; Lagazzo, A.; Crespo, M. A. R.; Escribano, V. S.; Busca, G.; *J. Catal.* **2014**, *311*, 102.
6. Morschbacker, A. J.; *J. Macromol. Sci., Polym. Rev.* **2009**, *49*, 79.
7. Moura, H. M.; Gibbons, N. L.; Miller, S.; Pastore, H. O.; *J. Catal.* **2018**, *362*, 129.
8. Gallo, J. M. R.; Schuchardt, U.; Bueno, J. M. C.; *J. Braz. Chem. Soc*. **2014**, *25*, 2229.
9. Favero, C.; Lima, D. W.; de Souza, R. F.; Bernardo-Gusmão, K.; *New J. Chem.* **2017**, *4*, 2333.
10. Zhang, M.; Yu, Y.; *Ind. Eng. Chem. Res.* **2013**, *52*, 9505.
11. Sheng, Q.; Ling, K.; Li, Z.; Zhao, L.; *Fuel Process. Technol.* **2013**, *110*, 73.
12. Takahara, I.; Saito, M.; Inaba, M.; Murata, K.; *Catal. Lett.* **2005**, *105*, 249.
13. Müller, J. M.; Mesquita, G. C.; Franco, S. M.; Borges, L. D.; Macedo, J. L.; Dias, J. A.; Dias, S. C. L.; *Microporous Mesoporous Mater.* **2015**, *204*, 50.
14. Pál-Bórbély, G.; Beyer, H. K.; *Phys. Chem. Chem. Phys.* **2003**, *5*, 2145.
15. Pires, J.; Carvalho, A.; Pinto, M.; Rocha, J.; *J. Porous Mater.* **2006**, *13*, 107.
16. Nash, C. P.; Ramanathan, A.; Ruddy, D. A.; Behl, M.; Gjersing, E.; Griffin, M.; Zhu, H.; Subramaniam, B.; Schaidle, J. A.; *Appl. Catal., A* **2016**, *510*, 110.
17. Hahn, C.; Füger, S.; Endisch, M.; Pacher, A.; Kureti, S.; *Catal. Commun.* **2015**, *58*, 108.
18. Sazama, P.; Wichterlová, B.; Sklenák, S.; Parvulescu, V. I.; Candu, N.; Sádovská, G.; Dědečeka, J.; Kleina, P.; Pashkovaa, V.; Šťastnýa, P.; *J. Catal.* **2014**, *318*, 22.
19. Rossetti, I.; Compagnoni, M.; Finocchio, E.; Ramis, G.; Di Michele, A.; Zucchini, A.; Dzwigaj, S.; *Int. J. Hydrogen Energy* **2016**, *41*, 16878.
20. Shahbazi, A.; Gonzalez-Olmos, R.; Kopinke, F.; Zarabadi-Poor, P.; Georgi, A.; *Sep. Purif. Technol.* **2014**, *127*, 1.
21. Wilson, W. B.; Costa, A. A.; Wang, H.; Campiglia, A. D.; Dias, J. A.; Dias, S. C. L.; *Microchem. J.* **2013**, *110*, 246.
22. Pillai, R. S.; Titus, E.; *Mater. Today: Proc.* **2015**, *2*, 446.
23. Dias, S. C. L.; Dias, J. A.; *Mol. Catal.* **2018**, *458*, 139.
24. Beyer, H. K.; Borbély-Pálné, G.; Wu, J.; *Stud. Surf. Sci. Catal.* **1994**, *84B*, 933.
25. Kollmer, F.; Hausmann, H. H. W. F.; *J. Catal.* **2004**, *227*, 398.
26. Phung, T. K.; Hernández, L. P.; Lagazzo, A.; Busca, G.; *Appl. Catal., A* **2015**, *493*, 77.
27. Catizzone, E.; Aloise, A.; Migliori, M.; Giordano, G.; *J. Energy Chem.* **2017**, *26*, 406.
28. Feliczak-Guzik, A.; *Microporous Mesoporous Mater.* **2018**, *259*, 33.
29. Feng, A.; Yu, Y.; Mi, L.; Cao, Y.; Yu, Y.; Song, L.; *Microporous Mesoporous Mater.* **2019**, *280*, 211.
30. Clemente, M. C. H.; *Martins*, G. A. V.; Freitas, E. F.; Dias, J. A.; Dias, S. C. L.; *Fuel* **2019**, *239*, 491.
31. Dömöka, M.; Tótha, M.; Raskób, J.; Erdohelyi, A.; *Appl. Catal., B* **2007**, *69*, 262.
32. Galvita, V. V.; Selmin, G. L.; Belyaev, V. D.; Semikolenova, V. A.; Tsiakarasb, P.; Sobyanin, V. A.; *Appl. Catal., A* **2001**, *220*, 123.
33. Fan, D.; Dai, D. J.; Wu, H. S.; *Materials* **2013**, *6*, 101.
34. Macedo, J. L.; Ghesti, G. F.; Dias, J. A.; Dias, S. C. L.; *Phys. Chem. Chem. Phys.* **2008**, *10*, 1584.
35. Braga, V. S.; Dias, J. A.; Dias, S. C. L.; Macedo, J. L.; *Chem. Mater.* **2005**, *17*, 690.
36. Freitas, E. F.; Araújo, A. A. L.; Paiva, M. F.; Dias, S. C. L.; Dias, J. A.; *Mol. Catal.* **2018**, *458*, 152.
37. Dias, J. A.; Dias, S. C. L.; Kob, N. E.; *J. Chem. Soc., Dalton Trans.* **2001**, 228.
38. Xu, S.; Sheng, H.; Ye, T.; Hu, D.; Liao, S.; *Catal. Commun.* **2016**, *78*, 75.

Submitted: February 1, 2019
Published online: May 23, 2019